algorithms

MDPI

Article

Poroelastic Medium with Non-Penetrating Crack Driven by Hydraulic Fracture: FEM Approximation Using HHT-α and Semi-Smooth Newton Methods

Victor A. Kovtunenko [1,*] and Olena M. Atlasiuk [2,3]

[1] Department of Mathematics and Scientific Computing, Karl-Franzens University of Graz, NAWI Graz, Heinrichstr. 36, 8010 Graz, Austria
[2] Institute of Mathematics, Czech Academy of Sciences, Žitná 25, 115 67 Prague, Czech Republic; hatlasiuk@gmail.com
[3] Department of Mathematics and Statistics, University of Helsinki, Pietari Kalmin katu 5, 00014 Helsinki, Finland
* Correspondence: victor.kovtunenko@uni-graz.at

Abstract

A new class of poroelastic dynamic contact problems stemming from hydraulic fracture theory is introduced and studied. The two-phase medium consists of a solid phase and pores which are saturated with a Newtonian fluid. The porous body contains a fluid-driven crack endowed with non-penetration conditions for the opposite crack surfaces. The poroelastic model is described by a coupled system of hyperbolic–parabolic partial differential equations under the unilateral constraint imposed on displacement. After full discretization using finite-element and Hilber–Hughes–Taylor methods, the well-posedness of the resulting variational inequality is established. Formulation of the complementarity conditions with the help of a minimum-based merit function is used for the semi-smooth Newton method of solution presented in the form of a primal–dual active set algorithm which is tested numerically.

Keywords: hydrofracking; Biot poroelasticity model; dynamic variational inequality; crack non-penetration; primal–dual active set

MSC: 35L85; 49M15; 74S05; 74R20

Academic Editor: Nargiz Sultanova

Received: 8 August 2025
Revised: 4 September 2025
Accepted: 11 September 2025
Published: 13 September 2025

Citation: Kovtunenko, V.A.; Atlasiuk, O.M. Poroelastic Medium with Non-Penetrating Crack Driven by Hydraulic Fracture: FEM Approximation Using HHT-α and Semi-Smooth Newton Methods. *Algorithms* **2025**, *18*, 579. https://doi.org/10.3390/a18090579

1. Introduction

In the current contribution, we present the mathematical modeling and finite-element approximation of a new class of dynamic contact problems for fluid-driven cracks introduced in [1–3]. These models describe hydraulic fractures subjected to non-penetration in geological reservoirs when mining oil and natural gas from the earth; see the overview of reservoir stimulation in hydraulic fracturing by [4]. We model the reservoir by a poroelastic medium consisting of two phases: solid particles and pores which are saturated with a Newtonian fluid. The two-phase body contains a single crack presenting the hydraulic fracture, which is created by pumping fracturing fluid into the well-bore, as drawn schematically in Figure 1. The novelty concerns inequality conditions at the crack preventing interpenetration of opposite crack surfaces. From a physical viewpoint, this allows for the compression of pressure such that the crack can close.

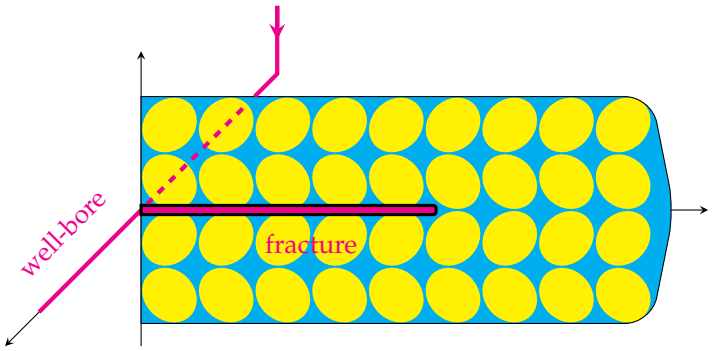

Figure 1. The right half of a fracture in reservoir.

The poroelastic problem consists of a dynamic system of coupled equations and inequalities for the unknown displacement in a solid, pressure in pores, and contact force under prescribed fluid pressure at the crack. Basic equations of motion for porous media were established by Biot [5] based on principles of soil mechanics; see [6,7]. For further development and applications of the poroelastic theory, we refer to [8–10], and to [11–13] for modeling aspects of a two-phase medium. From the mathematical viewpoint, the constitutive equations for poroelasticity are similar to the thermoelastic model when replacing pore pressure with temperature; see [14]. The problem of non-penetrating cracks in thermoelastic plates was solved in [15] using pseudo-monotone operator theory. In the literature, a quasi-static approximation of the Biot model is mostly considered by omitting the inertia term, whereas treatment of the full dynamic Biot system is more complicated and rare. In the variational form, the dynamic poroelastic problem implies a nonlinear evolution equation. The existence and uniqueness of a global strong solution was proved in [16] using the monotonicity method. The dynamic numerical solution was presented in [17].

Physical issues of dynamic fracture modeling are given in [18]. The Biot model describing hydraulic fractures in the poroelastic medium is developed in [19–21] and other works. We cite [22–24] for the phase-field approach to the geometric description of crack singularities. Finite element approximations of V-notches and star-shaped cracks with conventional stress-free faces were studied in [25,26]. For the variational theory of elastostatic models of solids with non-penetrating cracks we refer the readers to [27–31], and to [32] for its numerical treatment. Utilizing the penalty method, a poroelastic model accounting for non-penetration of crack faces was simulated in [33], and in [34] for shear fracture. For numerical solutions to complementarity problems, a semi-smooth Newton (SSN) method is advantageous because it has the locally super-linear rate and converges globally monotone; see [35]. It is based on a generalized gradient of non-smooth merit functions, for this reason, typically utilizing the minimum function. The SSN is realized in the form of a primal–dual active set (PDAS) algorithm. The PDAS strategy was applied to Signorini's contact problem with friction in [36,37], to dynamic frictional contact problem in [38], and to non-penetrating crack problems in [39,40]. When reducing the dual variable, the SSN can be reformulated as a purely primal Nitsche's method [41].

Suitable finite element (FEM), finite volume, and boundary element (BEM) methods can be found in [42–45]. FEM has historically been the method of choice for space–time formulations to tackle hyperbolic problems. However, recent advances in time-domain BEM such as [46,47] have significantly improved its applicability to dynamic elasticity. In the context of contact computational mechanics (see [48]), finite element approximation of elastodynamic contact problems was elaborated in [49]. The space semi-discretization is in general not stable with respect to the mechanical energy when decreasing the time step or increasing simulation time. To remedy well-posedness, a viscosity regularization is helpful; see [50–52]. For temporal (semi)discretization, the Hilber–Hughes–Taylor (HHT) scheme

is adopted in the literature [53]. We follow a generalized-α method [54] for $\alpha = 1 + \alpha_{\mathrm{HHT}}$. In the standard HHT-scheme, α_{HHT} is usually taken in the non-positive range $[-0.5, 0]$ to provide high-frequency dissipation. By this, the widely used schemes of the Newmark family can be described by two weight parameters γ, β, and $\alpha = 1$ (that is $\alpha_{\mathrm{HHT}} = 0$) as the particular case of HHT-α.

In the current contribution, in Section 2 we formulate the poroelastic dynamic contact problem for a crack subject to non-penetration constraint. Following [55,56], in Section 3 the corresponding FEM discretization in space and HHT-α scheme in time are introduced, and the existence of the variational solution to the fully discretized problem is proved rigorously. In Section 4 we present a PDAS algorithm based on SSN for the problem stated in the mixed primal–dual form and perform a numerical test in Section 5.

2. Setting of the Poroelastic Dynamic Contact Problem for Fluid-Driven Crack

For the geometric description, we assume that points $\mathbf{x} = (x_1, \dots, x_d) \in \mathbb{R}^d$, $d = 2, 3$, occupy a domain Ω with the Lipschitz boundary $\partial\Omega = \Gamma_{\mathrm{D}} \cup \Gamma_{\mathrm{N}}$ and outward normal $\mathbf{n} = (n_1, \dots, n_d)$. Let some surface Σ split Ω into two sub-domains Ω^+ and Ω^- with Lipschitz boundaries $\partial\Omega^+$ and $\partial\Omega^-$. By this, $\partial\Omega^+ \cap \partial\Omega^- = \Sigma$ and $\Omega = \Omega^+ \cup \Omega^- \cup \Sigma$ with the normal $\mathbf{n}$ at interface Σ outward to Ω^- and inward to Ω^+, see illustration in Figure 2. Let $\Gamma_{\mathrm{c}} \subset \Sigma$ be a portion of the interface with two opposite faces $\Gamma_{\mathrm{c}}^+ \subset \Sigma^+$ and $\Gamma_{\mathrm{c}}^- \subset \Sigma^-$. We denote by $\Omega_{\mathrm{c}} = \Omega \setminus \overline{\Gamma_{\mathrm{c}}}$ the domain with the crack. In the time $t \in [0, T)$, where the final time $T > 0$ is fixed, this determines the time-space cylinder $\Omega_{\mathrm{c}}^T = (0, T) \times \Omega_{\mathrm{c}}$ with the outer side $\partial\Omega^T = (0, T) \times \partial\Omega$ and surfaces $\Gamma_\gamma^T = (0, T) \times \Gamma_\gamma$ for the index $\gamma \in \{\mathrm{c}, \mathrm{D}, \mathrm{N}\}$.

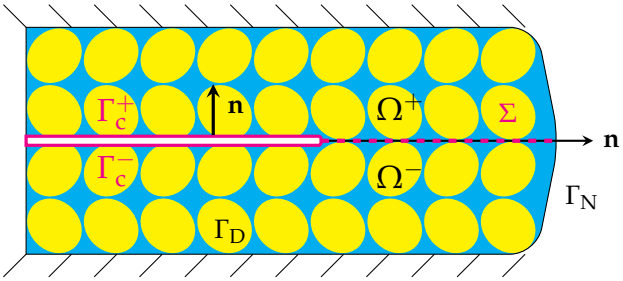

Figure 2. The poroelastic body with a crack in 2D.

In the solid phase, displacement field $\mathbf{u} = (u_1, \dots, u_d)(t, \mathbf{x})$ defines a 2nd-order symmetric tensor of linearized strain $\boldsymbol{\varepsilon} = \{\varepsilon_{ij}\}_{i,j=1}^d(t, \mathbf{x})$ with the entries

$$\varepsilon_{ij}(\mathbf{u}) = \frac{1}{2}\Big(\frac{\partial u_i}{\partial x_j} + \frac{\partial u_j}{\partial x_i}\Big), \quad i, j = 1, \dots, d. \tag{1}$$

Given a prestress $\boldsymbol{\tau}^0 = \{\tau_{ij}^0\}_{i,j=1}^d(\mathbf{x})$, the pore pressure field $p(t, \mathbf{x})$ and the 2nd-order symmetric tensor of Cauchy stress $\boldsymbol{\sigma} = \{\sigma_{ij}\}_{i,j=1}^d(t, \mathbf{x})$ compose the effective stress:

$$\boldsymbol{\tau} = \boldsymbol{\sigma}(\mathbf{u}) - ap\mathbf{I}, \quad \boldsymbol{\sigma}(\mathbf{u}) = \mathbf{A}\boldsymbol{\varepsilon}(\mathbf{u}) + \boldsymbol{\tau}^0 \tag{2}$$

with the 4th-order symmetric tensor $\mathbf{A} = \{A_{ijkl}\}_{i,j,k,l=1}^d$ of elastic coefficients $A_{ijkl} = A_{jikl} = A_{klij}$. In (2) the Biot coefficient $a \in (0, 1]$ and $\mathbf{I} \in \mathbb{R}^{d\times d}$ stands for the identity. Given the

volume force $\mathbf{f} = (f_1, \dots, f_d)(t, \mathbf{x})$, constant density of the elastic material $\rho > 0$, and the acceleration field $\ddot{\mathbf{u}}(t, \mathbf{x})$, the equation of motion reads component-wisely:

$$\rho \ddot{u}_i - \sum_{j=1}^{d} \frac{\partial \tau_{ij}}{\partial x_j} = f_i, \quad i = 1, \dots, d, \quad \text{in } \Omega_{\mathrm{c}}^T. \tag{3}$$

In pores, applying Fick's diffusion law and Stokes flow leads to the fluid mass balance:

$$S\dot{p} + a\,\mathrm{div}\dot{\mathbf{u}} - \kappa \Delta p = 0 \quad \text{in } \Omega_{\mathrm{c}}^T, \tag{4}$$

where $\dot{\mathbf{u}}(t, \mathbf{x})$ and $\dot{p}(t, \mathbf{x})$ are velocity fields, $S > 0$ denotes storativity, and the diffusion coefficient $\kappa = k_{\mathrm{r}}/\eta_{\mathrm{r}}$ employs permeability $k_{\mathrm{r}} > 0$ and effective viscosity $\eta_{\mathrm{r}} > 0$. The governing Equations (1)–(4) are supported by the initial conditions prescribed at $t = 0$:

$$\mathbf{u}(0, \cdot\,) = \mathbf{u}^0, \quad \dot{\mathbf{u}}(0, \cdot\,) = \dot{\mathbf{u}}^0, \quad p(0, \cdot\,) = p_{\mathrm{f}}(0, \cdot\,) \quad \text{in } \Omega_{\mathrm{c}}. \tag{5}$$

For given boundary force $\mathbf{g} = (g_1, \dots, g_d)(t, \mathbf{x})$ and pore pressure $p_{\mathrm{f}}(t, \mathbf{x})$ conforming (5) at $t = 0$, there are prescribed mixed boundary conditions at the outer side:

$$\mathbf{u} = \mathbf{0} \quad \text{on } \Gamma_{\mathrm{D}}^T, \quad \boldsymbol{\tau}\mathbf{n} = \mathbf{g} \quad \text{on } \Gamma_{\mathrm{N}}^T, \quad p = p_{\mathrm{f}} \quad \text{on } \partial\Omega^T. \tag{6}$$

Typically, leaving the Neumann portion empty is used to confine with Dirichlet conditions over the outer boundary $\partial\Omega^T$ stress and pressure measured in far-field. Contact conditions at the crack are derived below.

At Γ_{c} we decompose displacement and stress fields into tangential and normal components:

$$\mathbf{u} = u_n \mathbf{n} + \mathbf{u}_\Gamma, \; u_n := \mathbf{u} \cdot \mathbf{n}, \quad \boldsymbol{\tau}\mathbf{n} = \tau_n \mathbf{n} + \boldsymbol{\tau}\mathbf{n}_\Gamma, \; \tau_n := \boldsymbol{\tau}\mathbf{n} \cdot \mathbf{n},$$

where the dot implies the scalar product such that $\mathbf{u} \cdot \mathbf{n} = \sum_{i=1}^{d} u_i n_i$ and $\boldsymbol{\tau}\mathbf{n} \cdot \mathbf{n} = \sum_{i,j=1}^{d} \tau_{ij} n_i n_j$. The discontinuous fields allow a jump across the crack:

$$[\![\mathbf{u}]\!] := \mathbf{u}|_{\Gamma_{\mathrm{c}}^+} - \mathbf{u}|_{\Gamma_{\mathrm{c}}^-}, \quad [\![\boldsymbol{\tau}\mathbf{n}]\!] := \boldsymbol{\tau}\mathbf{n}|_{\Gamma_{\mathrm{c}}^+} - \boldsymbol{\tau}\mathbf{n}|_{\Gamma_{\mathrm{c}}^-}, \quad [\![p]\!] := p|_{\Gamma_{\mathrm{c}}^+} - p|_{\Gamma_{\mathrm{c}}^-}.$$

Let the pore pressure be prescribed at the opposite crack faces by $p_{\mathrm{f}}^+(t, \mathbf{x})$ and $p_{\mathrm{f}}^-(t, \mathbf{x})$ conforming (5) and (6) which can be different but should coincide at the crack tip. The fluid pressure is continuous over the crack, and friction-free contact respectively implies that

$$p = p_{\mathrm{f}}^{\pm}, \quad \boldsymbol{\tau}\mathbf{n}_\Gamma = \mathbf{0} \quad \text{on } \Gamma_{\mathrm{c}}^{T\pm}. \tag{7}$$

To prevent interpenetration between the opposite crack faces, we suggest unilateral contact conditions written in the complementary form:

$$[\![\tau_n + p]\!] = 0, \quad \tau_n + p \le 0, \quad [\![u_n]\!] \ge 0, \quad (\tau_n + p)[\![u_n]\!] = 0 \quad \text{on } \Gamma_{\mathrm{c}}^T. \tag{8}$$

Physically, conditions (8) imply compression for contact pressure allowing the crack to close.

To validate relations (1)–(8) in function spaces, we introduce the Sobolev space:

$$H_\omega^1(\Omega_{\mathrm{c}}) := \{v \in H^1(\Omega_{\mathrm{c}}) : \quad v = 0 \text{ a.e. } \omega\}, \quad \omega \in \{\Gamma_{\mathrm{D}}, \partial\Omega_{\mathrm{c}}\},$$

owing to the Dirichlet condition in (6) and (7), and the corresponding Bochner space

$$\mathcal{W}_\omega := \{v \in L^2(0, T; H_\omega^1(\Omega_{\mathrm{c}})), \quad \dot{v} \in L^2(0, T; L^2(\Omega_{\mathrm{c}}))\}.$$

Feasible displacement fields satisfying non-penetration in (8) build the convex closed cone:

$$\mathbf{K} = \{\mathbf{v} \in H^1_{\Gamma_\mathrm{D}}(\Omega_\mathrm{c})^d : \quad [\![v_n]\!] \geq 0 \text{ a.e. } \Gamma_\mathrm{c}\}.$$

Let forces $\mathbf{f} \in C([0,T]; L^2(\Omega_\mathrm{c})^d)$, $\mathbf{g} \in C([0,T]; L^2(\Gamma_\mathrm{N})^d)$, pressure $p_\mathrm{f} \in C([0,T]; L^2(\Omega_\mathrm{c}))$, prestress $\boldsymbol{\tau}^0 \in L^2(\Omega_\mathrm{c})^{d\times d}$, and initial fields in (5) satisfy $\mathbf{u}^0 \in \mathbf{K}$ with $[\![u^0_n]\!] = 0$, $\dot{\mathbf{u}}^0 \in L^2(\Omega_\mathrm{c})^d$.

For smooth tensor field $\boldsymbol{\tau}$ and vector field $\mathbf{v}$ the following Green's formula takes place:

$$-\sum_{i,j=1}^{d} \int_{\Omega_\mathrm{c}} \frac{\partial \tau_{ij}}{\partial x_j} v_i \, d\mathbf{x} = \int_{\Omega_\mathrm{c}} \boldsymbol{\tau} : \boldsymbol{\varepsilon}(\mathbf{v}) \, d\mathbf{x} - \int_{\partial\Omega} \boldsymbol{\tau}\mathbf{n} \cdot \mathbf{v} \, d\Gamma + \int_{\Gamma_\mathrm{c}} [\![\tau_n v_n + \boldsymbol{\tau}\mathbf{n}_\Gamma \cdot \mathbf{v}_\Gamma]\!] \, d\Gamma,$$

where ":" implies the double inner product. Testing it with $\mathbf{v} - \mathbf{u} \in H^1_{\Gamma_\mathrm{D}}(\Omega_\mathrm{c})^d$ after substitution of the equation of motion (1) and boundary conditions from (6)–(8) yields

$$\int_{\Omega_\mathrm{c}} \big((\rho\ddot{\mathbf{u}} - \mathbf{f}) \cdot (\mathbf{v} - \mathbf{u}) + \boldsymbol{\tau} : \boldsymbol{\varepsilon}(\mathbf{v} - \mathbf{u})\big) \, d\mathbf{x} + \int_{\Gamma_\mathrm{c}} [\![\tau_n (v_n - u_n)]\!] \, d\Gamma = \int_{\Gamma_\mathrm{N}} \mathbf{g} \cdot (\mathbf{v} - \mathbf{u}) \, d\Gamma. \quad (9)$$

Similarly, standard Green's formula for smooth scalar fields p and q:

$$-\int_{\Omega_\mathrm{c}} (\Delta p) q \, d\mathbf{x} = \int_{\Omega_\mathrm{c}} \nabla p \cdot \nabla q \, d\mathbf{x} - \int_{\partial\Omega_\mathrm{c}} (\nabla p \cdot \mathbf{n}) q \, d\Gamma$$

owing to the fluid mass balance Equation (4) follows when $q = 0$ at $\partial\Omega_\mathrm{c}$:

$$\int_{\Omega_\mathrm{c}} \big((S\dot{p} + a\mathrm{div}\dot{\mathbf{u}})q + \kappa \nabla p \cdot \nabla q\big) \, d\mathbf{x} = 0. \quad (10)$$

The integration of (9) and (10) by parts over time using initial conditions (5) and inequalities in (8) leads to the variational formulation of the dynamic poroelastic problem: Find $\mathbf{u} \in \mathcal{W}^d_{\Gamma_\mathrm{D}}$ with $\mathbf{u}(t, \cdot) \in \mathbf{K}$ for $t \in (0,T)$, $\mathbf{u}(0, \cdot) = \mathbf{u}^0$, and $p - p_\mathrm{f} \in \mathcal{W}_{\partial\Omega_\mathrm{c}}$ such that

$$\begin{aligned} &\int_{\Omega_\mathrm{c}^T} \big(-\rho\dot{\mathbf{u}} \cdot (\dot{\mathbf{v}} - \dot{\mathbf{u}}) + \boldsymbol{\tau} : \boldsymbol{\varepsilon}(\mathbf{v} - \mathbf{u})\big) \, d\mathbf{x}dt - \int_{\Gamma_\mathrm{c}^T} [\![p_\mathrm{f}(v_n - u_n)]\!] \, d\Gamma dt \\ &\qquad \geq \int_{\Omega_\mathrm{c}} \rho\dot{\mathbf{u}}^0 \cdot (\mathbf{v}(0, \cdot) - \mathbf{u}^0) \, d\mathbf{x} + \int_{\Omega_\mathrm{c}^T} \mathbf{f} \cdot (\mathbf{v} - \mathbf{u}) \, d\mathbf{x}dt + \int_{\Gamma_\mathrm{N}^T} \mathbf{g} \cdot (\mathbf{v} - \mathbf{u}) \, d\Gamma dt, \quad (11) \end{aligned}$$

$$\int_{\Omega_\mathrm{c}^T} \big((S\dot{p} + a\mathrm{div}\dot{\mathbf{u}})q + \kappa \nabla p \cdot \nabla q\big) \, d\mathbf{x}dt = 0, \quad (12)$$

for all $\mathbf{v} \in \mathcal{W}^d_{\Gamma_\mathrm{D}}$, $\mathbf{v}(t, \cdot) \in \mathbf{K}$ with $\mathbf{v} = \mathbf{u}$ for $t \geq T - \zeta$ at some $\zeta > 0$, and $q \in \mathcal{W}_{\partial\Omega_\mathrm{c}}$.

3. Full Discretization of the Dynamic Contact Problem

Let $\mathcal{T}_h$ be a regular quasi-uniform triangulation of the domain $\overline{\Omega}_\mathrm{c} = \cup_{K\in\mathcal{T}_h} \overline{K}$ with the mesh size $h > 0$. The FEM space is build by piecewise on $\mathcal{T}_h$ polynomials of degree $p \in \mathbb{N}$:

$$\mathcal{V}_{h\omega} = \big\{v_h \in C^0(\overline{\Omega}_\mathrm{c}) : \ v_h\big|_K \in \mathbb{P}_p(K) \text{ for all } K \in \mathcal{T}_h, \quad v_h = 0 \text{ on } \omega\big\}, \quad \omega \in \{\Gamma_\mathrm{D}, \partial\Omega_\mathrm{c}\}.$$

Let the triangulation be conformal to the subdivision of crack faces implying that the nodal points $\Gamma_\mathrm{c}^{h+} \subset \Gamma_\mathrm{c}^+$ and $\Gamma_\mathrm{c}^{h-} \subset \Gamma_\mathrm{c}^-$ coincide. Denoting the finite set $\Gamma_\mathrm{c}^h := \Gamma_\mathrm{c}^{h+} = \Gamma_\mathrm{c}^{h-}$ of cardinality $N_\mathrm{c}^h \in \mathbb{N}$ at the crack Γ_c, we look for the discrete contact force $\lambda_h = \tau_{hn} + p_h$ verifying complementarity conditions (8) on $\Gamma_{\mathrm{c}T}^h = (0,T) \times \Gamma_\mathrm{c}^h$. Let the FEM approximation of initial fields $\mathbf{u}_h^0 \in \mathcal{V}^d_{h\Gamma_\mathrm{D}}$, $\dot{\mathbf{u}}_h^0 \in \mathcal{V}^d_{h\varnothing}$, respectively $p_{\mathrm{f}h} \in \mathcal{V}_{h\varnothing}$. The semi-discretized in space variational inequality (11) and Equation (12) are expressed in the primal–dual form

as follows: Find displacement $\mathbf{u}_h : [0,T) \mapsto \mathcal{V}^d_{h\Gamma_\mathrm{D}}$ with $\mathbf{u}_h(0,\cdot) = \mathbf{u}^0_h$, $\dot{\mathbf{u}}_h(0,\cdot) = \dot{\mathbf{u}}^0_h$, pore pressure $p_h - p_{\mathrm{f}h} : [0,T) \mapsto \mathcal{V}_{h\partial\Omega_\mathrm{c}}$ with $p_h(0,\cdot) = p_{\mathrm{f}h}(0,\cdot)$, and $\lambda_h : [0,T) \mapsto \mathbb{R}^{N^h_\mathrm{c}}$ validating

$$[\![u_{hn}]\!] \geq 0, \quad \lambda_h \leq 0, \quad \lambda_h [\![u_{hn}]\!] = 0 \quad \text{on } \Gamma^h_{\mathrm{c}T}, \tag{13}$$

$$\int_{\Omega^T_\mathrm{c}} \left(\rho \ddot{\mathbf{u}}_h \cdot \mathbf{v}_h + \boldsymbol{\tau}_h : \boldsymbol{\varepsilon}(\mathbf{v}_h)\right) d\mathbf{x}dt + \int_{\Gamma^h_{\mathrm{c}T}} \lambda_h [\![v_{hn}]\!]\, d\Gamma dt = \int_{\Omega^T_\mathrm{c}} \mathbf{f} \cdot \mathbf{v}_h\, d\mathbf{x}dt + \int_{\Gamma^T_\mathrm{N}} \mathbf{g} \cdot \mathbf{v}_h\, d\Gamma dt + \int_{\Gamma^h_{\mathrm{c}T}} [\![p_{\mathrm{f}h} v_{hn}]\!]\, d\Gamma dt, \tag{14}$$

$$\int_{\Omega^T_\mathrm{c}} \left((S\dot{p}_h + a\mathrm{div}\dot{\mathbf{u}}_h) q_h + \kappa \nabla p_h \cdot \nabla q_h\right) d\mathbf{x}dt = 0, \tag{15}$$

for all test functions $\mathbf{v}_h \in C^0([0,T]; \mathcal{V}^d_{h\Gamma_\mathrm{D}})$ and $q_h \in C^0([0,T]; \mathcal{V}_{h\partial\Omega_\mathrm{c}})$.

Given $N \in \mathbb{N}$ and the step size $\tau = T/N$, consider uniform time-discretization of $[0,T]$ by points $t^m = m\tau$, $m = 0,\ldots,N$. Denote by $\mathbf{u}^m_h$, $\dot{\mathbf{u}}^m_h$, $\ddot{\mathbf{u}}^m_h$ the discrete displacement, velocity, acceleration, respectively, for the pore pressure p^m_h, $\dot{p}^m_h$, multiplier λ^m_h, and discrete forces $\mathbf{f}^m = \mathbf{f}(t^m,\cdot)$, $\mathbf{g}^m = \mathbf{g}(t^m,\cdot)$ at the time t^m. For $\alpha \in [0,1]$ we introduce the weighted sum:

$$\mathbf{v}^{m+\alpha}_h = \alpha \mathbf{v}^{m+1}_h + (1-\alpha)\mathbf{v}^m_h$$

for intermediate time steps $m+\alpha$. It is well-known that the 2nd-order consistent, standard Crank–Nicolson scheme is not stable for dynamic contact when decreasing step size. Given the Newmark parameters $\gamma \in [0,1]$ and $\beta \in [0,0.5]$, we realize the implicit Hilber–Hughes–Taylor (HHT-α) method from [54]. For $m \geq 0$ we fully discretize problem (13)–(15): Find $\mathbf{u}^{m+1}_h, \dot{\mathbf{u}}^{m+1}_h, \ddot{\mathbf{u}}^{m+1}_h \in \mathcal{V}^d_{h\Gamma_\mathrm{D}}$, $p^{m+1}_h - p_{\mathrm{f}h}, \dot{p}^{m+1}_h \in \mathcal{V}_{h\partial\Omega_\mathrm{c}}$, and $\lambda^{m+\alpha}_h \in \mathbb{R}^{N^h_\mathrm{C}}$ such that:

$$\mathbf{u}^{m+1}_h = \mathbf{u}^m_h + \tau\dot{\mathbf{u}}^m_h + \frac{\tau^2}{2}\ddot{\mathbf{u}}^{m+2\beta}_h, \quad \dot{\mathbf{u}}^{m+1}_h = \dot{\mathbf{u}}^m_h + \tau\ddot{\mathbf{u}}^{m+\gamma}_h, \quad p^{m+1}_h = p^m_h + \tau\dot{p}^{m+1}_h, \tag{16}$$

$$[\![u^{m+\alpha}_{hn}]\!] \geq 0, \quad \lambda^{m+\alpha}_h \leq 0, \quad \lambda^{m+\alpha}_h [\![u^{m+\alpha}_{hn}]\!] = 0 \quad \text{on } \Gamma^h_{\mathrm{c}T}, \tag{17}$$

$$\int_{\Omega_\mathrm{c}} \left(\rho \ddot{\mathbf{u}}^{m+1}_h \cdot \mathbf{v}_h + \boldsymbol{\tau}^{m+\alpha}_h : \boldsymbol{\varepsilon}(\mathbf{v}_h)\right) d\mathbf{x} + \int_{\Gamma^h_\mathrm{c}} \lambda^{m+\alpha}_h [\![v_{hn}]\!]\, d\Gamma = \int_{\Omega_\mathrm{c}} \mathbf{f}^{m+\alpha} \cdot \mathbf{v}_h\, d\mathbf{x} + \int_{\Gamma_\mathrm{N}} \mathbf{g}^{m+\alpha} \cdot \mathbf{v}_h\, d\Gamma + \int_{\Gamma^h_\mathrm{c}} [\![p^{m+\alpha}_{\mathrm{f}h} v_{hn}]\!]\, d\Gamma, \tag{18}$$

$$\int_{\Omega_\mathrm{c}} \left((S\dot{p}^{m+1}_h + a\mathrm{div}\dot{\mathbf{u}}^{m+1}_h) q_h + \kappa \nabla p^{m+1}_h \cdot \nabla q_h\right) d\mathbf{x} = 0, \tag{19}$$

for all test functions $\mathbf{v}_h \in \mathcal{V}^d_{h\Gamma_\mathrm{D}}$ and $q_h \in \mathcal{V}_{h\partial\Omega_\mathrm{c}}$. The acceleration may be initialized through

$$\int_{\Omega_\mathrm{c}} \left(\rho \ddot{\mathbf{u}}^0_h \cdot \mathbf{v}_h + \boldsymbol{\tau}^0_h : \boldsymbol{\varepsilon}(\mathbf{v}_h)\right) d\mathbf{x} = \int_{\Omega_\mathrm{c}} \mathbf{f}^0 \cdot \mathbf{v}_h\, d\mathbf{x} + \int_{\Gamma_\mathrm{N}} \mathbf{g}^0 \cdot \mathbf{v}_h\, d\Gamma + \int_{\Gamma^h_\mathrm{c}} [\![p^0_{\mathrm{f}h} v_{hn}]\!]\, d\Gamma.$$

Further, we prove the well-posedness of the problem (16)–(19). We recall the estimates for stress in (2): The constants $C_\mathrm{E}, C_\mathrm{K}, C_\mathrm{P}, C_\mathrm{I} > 0$ exist independent of h such that

$$\|\boldsymbol{\varepsilon}(\mathbf{v}_h)\|_{L^2(\Omega_\mathrm{c})} \leq \|\nabla \mathbf{v}_h\|_{L^2(\Omega_\mathrm{c})}, \quad \|\mathbf{A}\boldsymbol{\varepsilon}(\mathbf{v}_h)\|_{L^2(\Omega_\mathrm{c})} \leq C_\mathrm{E}\|\nabla \mathbf{v}_h\|_{L^2(\Omega_\mathrm{c})}, \tag{20}$$

the Korn and Poincaré inequalities yield:

$$\int_{\Omega_\mathrm{c}} \mathbf{A}\boldsymbol{\varepsilon}(\mathbf{v}_h) : \boldsymbol{\varepsilon}(\mathbf{v}_h)\, d\mathbf{x} \geq C_\mathrm{K}\|\mathbf{v}_h\|^2_{H^1(\Omega_\mathrm{c})}, \quad \int_{\Omega_\mathrm{c}} \kappa \nabla q_h \cdot \nabla q_h\, d\mathbf{x} \geq C_\mathrm{P}\|q_h\|^2_{H^1(\Omega_\mathrm{c})}, \tag{21}$$

and the inverse inequality holds:

$$\|\mathbf{v}_h\|_{L^2(\Omega_c)} \geq C_I h \|\mathbf{v}_h\|_{H^1(\Omega_c)}. \tag{22}$$

Theorem 1. *At each time-step m, the fully discrete mixed variational problem (16)–(19) admits the unique solution.*

Proof. Reducing the implicit acceleration and velocities by the mean of identities:

$$\dot{\mathbf{u}}_h^{m+1} = \frac{\gamma}{\beta\tau}(\mathbf{u}_h^{m+1} - \mathbf{u}_h^m) + (1 - \frac{\gamma}{\beta})\dot{\mathbf{u}}_h^m + \tau(1 - \frac{\gamma}{2\beta})\ddot{\mathbf{u}}_h^m, \quad \dot{p}_h^{m+1} = \frac{1}{\tau}(p_h^{m+1} - p_h^m),$$
$$\ddot{\mathbf{u}}_h^{m+1} = \frac{1}{\beta\tau^2}(\mathbf{u}_h^{m+1} - \mathbf{u}_h^m) - \frac{1}{\beta\tau}\dot{\mathbf{u}}_h^m + (1 - \frac{1}{2\beta})\ddot{\mathbf{u}}_h^m, \tag{23}$$

the HHT system can be rewritten with respect to $\mathbf{u}_h^{m+\alpha}$, $p_h^{m+\alpha}$, and $\lambda_h^{m+\alpha}$ in the explicit form:

$$[\![u_{hn}^{m+\alpha}]\!] \geq 0, \quad \lambda_h^{m+\alpha} \leq 0, \quad \lambda_h^{m+\alpha}[\![u_{hn}^{m+\alpha}]\!] = 0 \quad \text{on } \Gamma_{cT}^h, \tag{24}$$

$$\mathbf{A}_\tau(\mathbf{u}_h^{m+\alpha}, \mathbf{v}_h) - \int_{\Omega_c} a p_h^{m+\alpha} \mathrm{div}\mathbf{v}_h \, d\mathbf{x} + \int_{\Gamma_c^h} \lambda_h^{m+\alpha}[\![v_{hn}]\!] \, d\Gamma = \mathbf{F}_\tau^m(\mathbf{v}_h), \tag{25}$$

$$B_\tau(p_h^{m+\alpha}, q_h) + \int_{\Omega_c} \frac{a}{\tau} \mathrm{div}\mathbf{u}_h^{m+\alpha} q_h \, d\mathbf{x} = G_\tau^m(q_h), \tag{26}$$

for all test functions $\mathbf{v}_h \in \mathcal{V}_{h\Gamma_D}^d$ and $q_h \in \mathcal{V}_{h\partial\Omega_c}$, with bilinear operators $\mathbf{A}_\tau : \mathcal{V}_{h\Gamma_D}^d \times \mathcal{V}_{h\Gamma_D}^d \mapsto \mathbb{R}$ and $B_\tau : \mathcal{V}_{h\partial\Omega_c} \times \mathcal{V}_{h\partial\Omega_c} \mapsto \mathbb{R}$ in the left-hand side of (25) and (26):

$$\mathbf{A}_\tau(\mathbf{u}_h^{m+\alpha}, \mathbf{v}_h) := \int_{\Omega_c} \Big(\frac{\rho}{\alpha\beta\tau^2} \mathbf{u}_h^{m+\alpha} \cdot \mathbf{v}_h + \mathbf{A}\boldsymbol{\varepsilon}(\mathbf{u}_h^{m+\alpha}) : \boldsymbol{\varepsilon}(\mathbf{v}_h) \Big) d\mathbf{x},$$
$$B_\tau(p_h^{m+\alpha}, q_h) := \int_{\Omega_c} \Big(\frac{S}{\tau} p_h^{m+\alpha} q_h + \kappa \nabla p_h^{m+\alpha} \cdot \nabla q_h \Big) d\mathbf{x}$$

and linear operators $\mathbf{F}_\tau^m : \mathcal{V}_{h\Gamma_D}^d \mapsto \mathbb{R}$ and $G_\tau^m : \mathcal{V}_{h\partial\Omega_c} \mapsto \mathbb{R}$ in the right-hand side:

$$\mathbf{F}_\tau^m(\mathbf{v}_h) := \int_{\Omega_c} \Big\{ \Big[\mathbf{f}^{m+\alpha} + \frac{\rho}{\beta\tau^2} \Big(\frac{1}{\alpha}\mathbf{u}_h^m + \tau\dot{\mathbf{u}}_h^m + \tau^2(\frac{1}{2} - \beta)\ddot{\mathbf{u}}_h^m \Big) \Big] \cdot \mathbf{v}_h - \boldsymbol{\tau}^0 : \boldsymbol{\varepsilon}(\mathbf{v}_h) \Big\} d\mathbf{x}$$
$$+ \int_{\Gamma_N} \mathbf{g}^{m+\alpha} \cdot \mathbf{v}_h \, d\Gamma + \int_{\Gamma_c^h} [\![p_{fh}^{m+\alpha} v_{hn}]\!] \, d\Gamma,$$
$$G_\tau^m(q_h) := \int_{\Omega_c} \Big(\frac{1}{\tau}(S p_h^m + a\mathrm{div}\mathbf{u}_h^m) + (\alpha - 1)(S\dot{p}_h^m + a\mathrm{div}\dot{\mathbf{u}}_h^m) \Big) q_h \, d\mathbf{x}.$$

The summation of (25) with (26) multiplied by τ yields a single equation for the solution pair $(\mathbf{u}_h^{m+\alpha}, p_h^{m+\alpha})$ and builds a bilinear from in the left-hand side which is coercive:

$$\mathbf{A}_\tau(\mathbf{u}_h^{m+\alpha}, \mathbf{u}_h^{m+\alpha}) + \tau B_\tau(p_h^{m+\alpha}, p_h^{m+\alpha})$$
$$\geq (\frac{\rho h^2 C_I^2}{\alpha\beta\tau^2} + C_K) \|\mathbf{u}_h^{m+\alpha}\|_{H^1(\Omega_c)}^2 + (Sh^2 C_I^2 + \tau C_P) \|p_h^{m+\alpha}\|_{H^1(\Omega_c)}^2,$$

because the mixed terms are canceled, and using the norm estimates (13)–(15). Therefore, reducing $\lambda_h^{m+\alpha}$ from the problem (24)–(26) it implies a variational inequality with the coercive bounded bilinear operator subjected to the inequality constraint in the cone $\mathbf{K}$, thus has the unique solution according to the Lions–Stampacchia theorem. The proof is finished. □

4. Semi-Smooth Newton Method for the Solution of the Mixed Variational Problem

For arbitrary constant $r > 0$ we introduce a merit function arising as the minimum:

$$\Phi : \mathbb{R}^2 \mapsto \mathbb{R}, \quad \Phi(\xi, \eta) := \min(\xi, -r\eta).$$

The complementarity conditions (24) can be expressed equivalently as the nonlinear equation:

$$\Phi([\![u_{hn}^{m+\alpha}]\!], \lambda_h^{m+\alpha}) = 0 \quad \text{on } \Gamma_{cT}^h. \tag{27}$$

Rewriting (27) in the following way: $r\lambda_h^{m+\alpha} = \min([\![u_{hn}^{m+\alpha}]\!] + r\lambda_h^{m+\alpha}, 0)$, we split the contact set Γ_c^h into the strictly active set of nodes:

$$\mathcal{A}([\![u_{hn}^{m+\alpha}]\!], \lambda_h^{m+\alpha}) := \{\mathbf{x} \in \Gamma_c^h : \ ([\![u_{hn}^{m+\alpha}]\!] + r\lambda_h^{m+\alpha})(\mathbf{x}) < 0\}, \tag{28}$$

and its complementary inactive set:

$$\mathcal{I}([\![u_{hn}^{m+\alpha}]\!], \lambda_h^{m+\alpha}) := \{\mathbf{x} \in \Gamma_c^h : \ ([\![u_{hn}^{m+\alpha}]\!] + r\lambda_h^{m+\alpha})(\mathbf{x}) \geq 0\}, \tag{29}$$

such that

$$[\![u_{hn}^{m+\alpha}]\!] = 0 \text{ on } \mathcal{A}([\![u_{hn}^{m+\alpha}]\!], \lambda_h^{m+\alpha}), \quad \lambda_h^{m+\alpha} = 0 \text{ on } \mathcal{I}([\![u_{hn}^{m+\alpha}]\!], \lambda_h^{m+\alpha}). \tag{30}$$

For the solution of the primal–dual system (24)–(26), we perform the semi-smooth Newton method as a primal–dual active set (PDAS) algorithm based on formalism (28)–(30).

1. Initialization:

Initialize $\mathcal{A}_h^{-1} \subset \Gamma_c^h$ with some guesses.

2. Iteration step:

At every iterate $k \geq -1$, solve the successive linear problem with respect to the triple $(\mathbf{u}_h^{m+\alpha,k+1}, p_h^{m+\alpha,k+1} - p_{fh}, \lambda_h^{m+\alpha,k+1}) \in \mathcal{V}_{h\Gamma_D}^d \times \mathcal{V}_{h\partial\Omega_c} \times \mathbb{R}^{N_c^h}$, which validates:

$$[\![u_{hn}^{m+\alpha,k+1}]\!] = 0 \text{ on } \mathcal{A}_h^k, \quad \lambda_h^{m+\alpha,k+1} = 0 \text{ on } \mathcal{I}_h^k, \tag{31}$$

$$\mathbf{A}_\tau(\mathbf{u}_h^{m+\alpha,k+1}, \mathbf{v}_h) - \int_{\Omega_c} a p_h^{m+\alpha,k+1} \mathrm{div}\mathbf{v}_h \, d\mathbf{x} + \int_{\Gamma_c^h} \lambda_h^{m+\alpha,k+1} [\![v_{hn}]\!] \, d\Gamma = \mathbf{F}_\tau^m(\mathbf{v}_h), \tag{32}$$

$$B_\tau(p_h^{m+\alpha,k+1}, q_h) + \int_{\Omega_c} \frac{a}{\alpha\tau} \mathrm{div}\mathbf{u}_h^{m+\alpha,k+1} q_h \, d\mathbf{x} = G_\tau^m(q_h), \tag{33}$$

for all test functions $\mathbf{v}_h \in \mathcal{V}_{h\Gamma_D}^d$ and $q_h \in \mathcal{V}_{h\partial\Omega_c}$

3. Iteration step:

Compute the complementary active and inactive sets:

$$\mathcal{A}^{k+1} = \{\mathbf{x} \in \Gamma_c^h : \ ([\![u_{hn}^{m+\alpha,k+1}]\!] + r\lambda_h^{m+\alpha,k+1})(\mathbf{x}) < 0\},$$
$$\mathcal{I}^{k+1} = \{\mathbf{x} \in \Gamma_c^h : \ ([\![u_{hn}^{m+\alpha,k+1}]\!] + r\lambda_h^{m+\alpha,k+1})(\mathbf{x}) \geq 0\}. \tag{34}$$

4. Stopping rule:

If $\mathcal{A}^{k+1} = \mathcal{A}^k$, then stop with the exact solution to the problem (25), (26), (28)–(30):

$$(\mathbf{u}_h^{m+\alpha}, p_h^{m+\alpha}, \lambda_h^{m+\alpha}) = (\mathbf{u}_h^{m+\alpha,k+1}, p_h^{m+\alpha,k+1}, \lambda_h^{m+\alpha,k+1}).$$

From the property of coercivity of the bilinear form established in the proof of Theorem 1, it follows straightforwardly the unique solution to the Newton iterate (31)–(33) at each k.

5. Numerical Test

For computer simulation, we choose the following geometry given in meters in 2D:

$$\Omega^- = \{\mathbf{x} \in (0, 2.5) \times (0, 1)\}, \quad \Omega^+ = \{\mathbf{x} \in (0, 2.5) \times (1, 2)\},$$
$$\Gamma_{\mathrm{D}} = \partial\Omega, \quad \Gamma_{\mathrm{N}} = \emptyset, \quad \Gamma_{\mathrm{c}} = \{x_2 = 1\}.$$

The parameters are, for the isotropic solid: material density $\rho = 2700$ [kg/m^3], Young modulus $E = 73$ [GPa] and Poisson ratio $\nu = 0.34$ yielding the shear modulus $\mu = E/(2(1+\nu)) \approx 27$ [GPa]; for fluid: storativity $S = 0.0146$ [1/GPa], diffusion coefficient $\kappa = 0.01$ [m^2/(GP×s)], and Biot coefficient $a = 0.75$. We test the poroelastic body which is uniformly compressed with the body force $\mathbf{f} = (0, 50)$ [kN] in Ω^-, and $\mathbf{f} = (0, -50)$ [kN] in Ω^+, such that the crack is closed.

The fluid pressure at the crack is prescribed by a piecewise-linear "hat" function:

$$p_{\mathrm{f}} = \frac{8\mu}{T} t x_1 \text{ for } x_1 \in (0, 1.25], \quad p_{\mathrm{f}} = \frac{8\mu}{T} t(2.5 - x_1) \text{ for } x_1 \in (1.25, 2.5)$$

for loading as $t \in [0, T/2)$, and respective unloading as $t \in [T/2, T]$:

$$p_{\mathrm{f}} = \frac{8\mu}{T}(T - t)x_1 \text{ for } x_1 \in (0, 1.25), \quad p_{\mathrm{f}} = \frac{8\mu}{T}(T - t)(2.5 - x_1) \text{ for } x_1 \in [1.25, 2.5).$$

The initial data are velocity $\dot{\mathbf{u}}^0 = \mathbf{0}$, acceleration $\ddot{\mathbf{u}}^0 = \mathbf{0}$, and $p_{\mathrm{f}} = 0$ on Γ_{D}. We utilize the standard piecewise $\mathbb{P}_1$-polynomial FEM for $\mathcal{V}_h$. In Figure 3, the loading–unloading loop is shown at time $t^m = m\tau$, $m = 0, \ldots, 8$ in the current configuration $\mathbf{x} + \mathbf{u}_h^m$ for grid points $\mathbf{x}_h \in \Omega_{\mathrm{c}}$ with the mesh size $h = 0.1$ [m] and step size $\tau = 0.625$ [s]. The corresponding pore pressure p_h^m calculated for $m = 0, \ldots, 8$ in the domain with crack Ω_{c} is depicted in Figure 4.

To examine the stability of the discrete dynamic contact problem, let us consider the energy:

$$E_h^m := \frac{1}{2} \int_{\Omega_{\mathrm{c}}} \left(\rho |\dot{\mathbf{u}}_h^m|^2 + S(p_h^m)^2 + \mathbf{A}\boldsymbol{\varepsilon}(\mathbf{u}_h^m) : \boldsymbol{\varepsilon}(\mathbf{u}_h^m) + \kappa \nabla p_h^m \cdot \nabla p_h^m \right) d\mathbf{x}, \tag{35}$$

for $m = 0, \ldots, N$. We compare the discrete energy E_h^m computed by (35) for three different HHT-α schemes: the standard Cranck–Nicolson (CN) scheme [$\gamma = 0.5$, $\beta = 0.25$, $\alpha = 1$], the fully implicit Newmark scheme [$\gamma = 1, \beta = 0.5, \alpha = 1$], and the HHT scheme [$\gamma = 0.6, \beta = 0.3025, \alpha = 0.9$]. The particular choice $\alpha = 0.9$ corresponds to the family of schemes $\alpha_{\mathrm{HHT}} = -0.1$ taken from [53]. The result is given in [MJ] as presented with solid lines during the time $T = 5$ [s] in the three corresponding rows (a), (b), and (c) of Figure 5. In each row, three different plots are related to time steps $\tau \in \{9, 18, 35\}$ [ms] at fixed $h = 5$ [cm]. For comparison, dashed curves present filtered data $E_{h,\mathrm{filtered}}^m$ obtained with the filter command in Matlab. From experiments, we report that the numerical scheme may become unstable when the step size drops, and moderate oscillations appear. The jumps in the energy take place at the initial time $t = 0$ of crack nucleation, as marked by crosses in Figure 5.

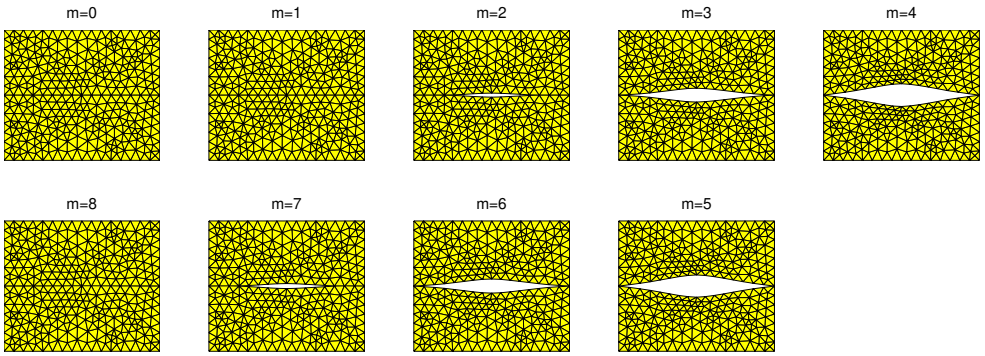

Figure 3. Displacement fields in the reference configuration $\mathbf{x} + \mathbf{u}_h^m$, $m = 0, \ldots, 8$.

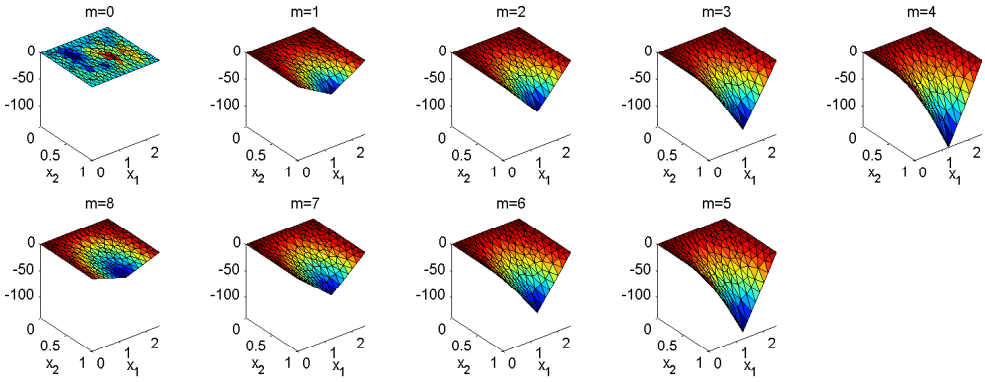

Figure 4. Pore-pressure fields p_h^m [GPa] in Ω_c, $m = 0, \ldots, 8$.

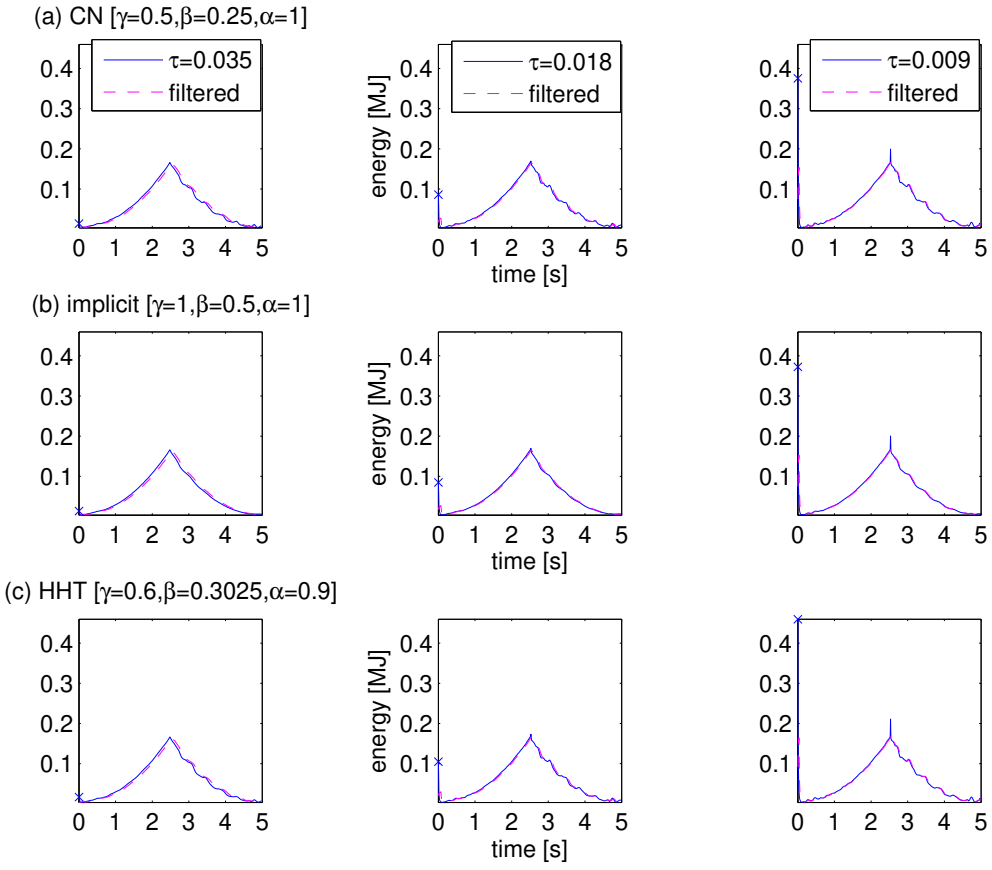

Figure 5. Discrete energy E_h^m versus time t^m for selected $[\gamma, \beta, \alpha]$ by decreasing τ.

For $t > 0$, Table 1 compares numerical oscillation amplitudes:

$$O_\tau := \max_{m=1,\dots,N} |E_h^m - E_{h,\text{filtered}}^m| \tag{36}$$

computed for the three HHT-α schemes in dependence of time-step sizes.

Table 1. Oscillation amplitudes O_τ across step sizes τ.

Scheme:	$\tau = 0.035$	$\tau = 0.018$	$\tau = 0.009$
$[\gamma = 0.5, \beta = 0.25, \alpha = 1]$	0.0141	0.0230	0.1196
$[\gamma = 1, \beta = 0.5, \alpha = 1]$	0.0117	0.0229	0.1181
$[\gamma = 0.6, \beta = 0.3025, \alpha = 0.9]$	0.0138	0.0255	0.1318

For the iterative solution of the discrete problems, we realize the semi-smooth Newton iteration in the form of the PDAS algorithm stated between the lines (31)–(34). The typical behavior starting with $\mathcal{A}^{-1} = \emptyset$ and $r = 1$ is demonstrated for the intermediate time $m = 17$ in Figure 6. The spatial system has 16194 unknowns as $h = 0.02$, and 90 time steps for $\tau = 0.055$. The crack opening $[\![u_{hn}^{m,k}]\!]$, Lagrange multiplier $\lambda_h^{m,k}$, and active set $\mathcal{A}^k$ are depicted at $N_c^h = 90$ points along the discretized crack Γ_c^h. The algorithm converges in only five iterations at the exact solution of the poroelastic contact problem (16)–(19). From Figure 6 we can justify a monotone and super-liner convergence of the semi-smooth Newton iterates.

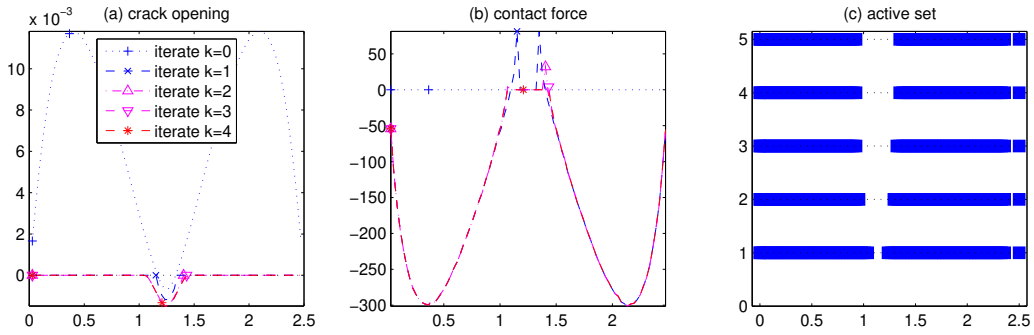

Figure 6. PDAS iterates k: crack opening $[\![u_{hn}^{m,k}]\!]$; contact force $\lambda_h^{m,k}$; active set $\mathcal{A}^k$ (in the blue color).

Table 2 presents computational efficiency for the PDAS algorithm in dependence of step sizes: number of constraints, maximal number of iterations, and CPU time in seconds pro iteration, observed in experiments and presented at selected times for the HHT scheme $[\gamma = 0.6, \beta = 0.3025, \alpha = 0.9]$.

Table 2. Computational efficiency of PDAS across step sizes.

Step-Size τ	**Constraints**	**Iterations**	**CPU Times**
0.312	15	5	0.0018
0.138	35	4	0.0199
0.092	53	4	0.0560
0.070	70	5	0.1518
0.056	88	4	0.1815

6. Conclusions

In the current contribution, the primal–dual active set algorithm is justified within time-integration schemes based on the Hilber–Hughes–Taylor method. It is applied to the dynamic variational inequality describing non-penetrating fractures in poroelastic

reservoirs. For further developments in the field of fracture applications, we cite the nonlinear modeling of a porous body with a fluid-driven crack under cohesion contact conditions and fluid volume control [57]. In the context of an algorithmic solution of dynamic contact problems, future research directions concern full space–time finite-element approximation matching discontinuous velocities; see the recent concept [58,59].

Author Contributions: Conceptualization, V.A.K.; writing—review and editing, O.M.A. All authors have read and agreed to the published version of the manuscript.

Funding: The work is supported by the Danube multilateral project in the frame of OeAD Scientific & Technological Cooperation (MULT 06/2023) financed by Austrian Federal Ministry of Science, Research and Economy (BMWFW); and by Czech Ministry of Education, Youth and Sports (MŠMT project 8X23001). V.A.K. acknowledges the financial support by the University of Graz. O.M.A. is financially supported by the Academy of Finland grant no. 367369.

Data Availability Statement: Data is contained within the article.

Conflicts of Interest: The authors declare no conflicts of interest.

References

1. Itou, H.; Kovtunenko, V.A.; Lazarev, N.P. Poroelastic problem of a non-penetrating crack with cohesive contact for fluid-driven fracture. *Appl. Eng. Sci.* **2023**, *15*, 100136. [CrossRef]
2. Kovtunenko, V. Poroelastic medium with a non-penetrating crack driven by hydraulic fracture: Variational inequality and its semidiscretization. *J. Comput. Optim. Appl.* **2022**, *405*, 113953. [CrossRef]
3. Kovtunenko, V.; Lazarev, N. The energy release rate for non-penetrating crack in poroelastic body driven by hydraulic fracture. *Math. Mech. Solids* **2023**, *28*, 592–610. [CrossRef] [PubMed]
4. Economides, M.; Nolte, K. (Eds.) *Reservoir Stimulation*; Wiley: Chichester, UK, 2000.
5. Biot, M. Theory of propagation of elastic waves in a fluid saturated porous solid. I and II. *J. Acoust. Soc. Am.* **1956**, *28*, 168–191. [CrossRef]
6. Coussy, O. *Poromechanics*; Wiley: Chichester, UK, 2004. [CrossRef]
7. Terzaghi, K. *Theoretical Soil Mechanics*; Wiley: New York, NY, USA, 1943. [CrossRef]
8. Barenblatt, G.; Zheltov, I.; Kochina, I. Basic concepts in the theory of seepage of homogeneous liquids in fissured rocks. *J. Appl. Math. Mech.* **1960**, *24*, 1286–1303. [CrossRef]
9. Khristianovic, S.; Zheltov, Y. Formation of vertical fractures by means of highly viscous fluids. In Proceedings of the 4th World Petroleum Congress, Rome, Italy, 6–15 June 1955; Volume II, pp. 579–586.
10. Meirmanov, A. *Mathematical Models for Poroelastic Flows*; Atlantis Press: Paris, France, 2014. [CrossRef]
11. Alekseev, G.; Spivak, Y.; Yashchenko, E. Theoretical analysis of the 2D thermal cloaking problem. *J. Phys. Conf. Ser.* **2017**, *803*, 012001. [CrossRef]
12. Antontsev, S.; Kuznetsov, I.; Sazhenkov, S.; Shmarev, S. Solutions of impulsive $p(x,t)$-parabolic equations with an infinitesimal initial layer. *Nonlinear Anal. Real World Appl.* **2024**, *80*, 104162. [CrossRef]
13. Kovtunenko, V.; Zubkova, A. Mathematical modeling of a discontinuous solution of the generalized Poisson–Nernst–Planck problem in a two-phase medium. *Kinet. Relat. Mod.* **2018**, *11*, 119–135. [CrossRef]
14. Rudoy, E.M.; Sazhenkov, S.A. The homogenized dynamical model of a thermoelastic composite stitched with reinforcing filaments. *Phil. Trans. R. Soc. A* **2024**, *382*, 20230304. [CrossRef]
15. Hoffmann, K.H.; Khludnev, A. On cracks of minimal opening in thermoelastic plates. *Z. Angew. Math. Mech.* **2000**, *80*, 253–258. [CrossRef]
16. Showalter, R.; Stefanelli, U. Diffusion in poro-plastic media. *Math. Meth. Appl. Sci.* **2004**, *27*, 2131–2151. [CrossRef]
17. Zienkiewicz, O.; Shiomi, T. Dynamic behaviour of saturated porous media; the generalized Biot formulation and its numerical solution. *Int. J. Numer. Anal. Methods Geomech.* **1984**, *8*, 71–96. [CrossRef]
18. Bratov, V.; Morozov, N.; Petrov, Y. *Dynamic Strength of Continuum*; St. Petersburg University: Saint Petersburg, Russia , 2009.
19. Bunger, A.; Detournay, E.; Garagash, D. Toughness-dominated hydraulic fracture with leak-off. *Int. J. Fract.* **2005**, *134*, 175–190. [CrossRef]
20. Peirce, A.; Detournay, E. An implicit level set method for modeling hydraulically driven fractures. *Comput. Methods Appl. Mech. Eng.* **2008**, *197*, 2858–2885. [CrossRef]
21. Shelukhin, V.; Baikov, V.; Golovin, S.; Davletbaev, A.; Starovoitov, V. Fractured water injection wells: Pressure transient analysis. *Int. J. Solids Struct.* **2014**, *51*, 2116–2122. [CrossRef]

22. Borden, M.; Verhoosel, C.; Scott, M.; Hughes, T.; Landis, C. A phase-field description of dynamic brittle fracture. *Comput. Methods Appl. Mech. Eng.* **2012**, *217–220*, 77–95. [CrossRef]
23. Mikayelyan, H. Some recent results on regularity of the crack-tip/crack-front of Mumford–Shah minimizers. In *Mathematical Analysis of Continuum Mechanics and Industrial Applications III: Proceedings of the International Conference CoMFoS18*; Itou, H., Hirano, S., Kimura, M., Kovtunenko, V., Khludnev, A., Eds.; Springer: Singapore, 2020; pp. 23–33. [CrossRef]
24. Mikelić, A.; Wheeler, M.; Wick, T. A phase-field method for propagating fluid-filled fractures coupled to a surrounding porous medium. *SIAM Multiscale Model. Simul.* **2015**, *13*, 367–398. [CrossRef]
25. Mallikarjunaiah, M.; Gou, K. Crack-tip field characterization in nonlinearly constituted and geometrically linear elastoporous solid containing a star-shaped crack: A finite element study. *arXiv* **2025**, arXiv:2507.09263. [CrossRef]
26. Shylaja, G.; Naidu, V.K.; Venkatesh, B.; Mallikarjunaiah, M. Finite element modeling of V-notched thermoelastic strain-limiting solids containing inclusions. *arXiv* **2025**, arXiv:2507.09300. [CrossRef]
27. Bach, M.; Khludnev, A.; Kovtunenko, V. Derivatives of the energy functional for 2D-problems with a crack under Signorini and friction conditions. *Math. Meth. Appl. Sci.* **2000**, *23*, 515–534. [CrossRef]
28. Khludnev, A.; Kovtunenko, V. *Analysis of Cracks in Solids*; Volume 6: Advances in Fracture Mechanics Series; WIT-Press: Southampton, UK; Boston, MA, USA, 2000.
29. Khludnev, A.M.; Kovtunenko, V.A.; Tani, A. Evolution of a crack with kink and non-penetration. *J. Math. Soc. Jpn.* **2008**, *60*, 1219–1253. [CrossRef]
30. Khludnev, A.; Sokołowski, J. Griffith formulae for elasticity systems with unilateral conditions in domains with cracks. *Eur. J. Mech. A Solids* **2000**, *19*, 105–119. [CrossRef]
31. Popova, T. The problem on T-shape junction of thin inclusions. *Sib. Electron. Math. Rep.* **2024**, *21*, 1578–1593. [CrossRef]
32. Kovtunenko, V. Numerical simulation of the non-linear crack problem with non-penetration. *Math. Meth. Appl. Sci.* **2004**, *27*, 163–179. [CrossRef]
33. Baykin, A.; Golovin, S. Modelling of hydraulic fracture propagation in inhomogeneous poroelastic medium. *J. Phys. Conf. Ser.* **2016**, *722*, 012003. [CrossRef]
34. Amor, H.; Marigo, J.J.; Maurini, C. Regularized formulation of the variational brittle fracture with unilateral contact: Numerical experiments. *J. Mech. Phys. Solids* **2017**, *57*, 1209–1229. [CrossRef]
35. Hintermüller, M.; Ito, K.; Kunisch, K. The primal-dual active set strategy as a semismooth Newton method. *SIAM J. Optim.* **2002**, *13*, 865–888. [CrossRef]
36. Hüeber, S.; Stadler, G.; Wohlmuth, B. A primal-dual active set algorithm for three-dimensional contact problems with Coulomb friction. *SIAM J. Sci. Comput.* **2008**, *30*, 572–596. [CrossRef]
37. Kučera, R.; Motyčková, K.; Markopoulos, A.; Haslinger, J. On the inexact symmetrized globally convergent semi-smooth Newton method for 3D contact problems with Tresca friction: The R-linear convergence rate. *Optim. Methods Softw.* **2020**, *35*, 65–86. [CrossRef]
38. Abide, S.; Barboteu, M.; Cherkaoui, S.; Dumont, S. Unified primal-dual active set method for dynamic frictional contact problems. *Fixed Point Theory Algorithms Sci. Eng.* **2022**, *2022*, 19. [CrossRef]
39. Hintermüller, M.; Kovtunenko, V.A.; Kunisch, K. Generalized Newton methods for crack problems with non-penetration condition. *Numer. Meth. Partial Differ. Equ.* **2005**, *21*, 586–610. [CrossRef]
40. Hintermüller, M.; Kovtunenko, V.; Kunisch, K. A Papkovich–Neuber-based numerical approach to cracks with contact in 3D. *IMA J. Appl. Math.* **2009**, *74*, 325–343. [CrossRef]
41. Chouly, F.; Hild, P.; Renard, Y. A Nitsche finite element method for dynamic contact: 1 and 2. *ESAIM Math. Model. Numer. Anal.* **2015**, *49*, 481–528. [CrossRef]
42. Bause, M.; Radu, F.; Köcher, U. Space–time finite element approximation of the Biot poroelasticity system with iterative coupling. *Comput. Methods Appl. Mech. Eng.* **2017**, *320*, 745–768. [CrossRef]
43. Gwinner, J.; Stephan, E.P. *Advanced Boundary Element Methods. Treatment of Boundary Value, Transmission and Contact Problems*; Springer: Cham, Switzerland, 2018. [CrossRef]
44. Linck, V.; Bayada, G.; Baillet, L.; Sassi, T.; Sabil, J. Finite element analysis of a contact with friction between an elastic body and a thin soft layer. *J. Tribol.* **2005**, *127*, 461–468. [CrossRef]
45. Mikelić, A.; Wang, B.; Wheeler, M. Numerical convergence study of iterative coupling for coupled flow and geomechanics. *Comput. Geosci.* **2014**, *18*, 325–341. [CrossRef]
46. Aimi, A.; Dallospedale, S.; Desiderio, L.; Guardasoni, C. A space–time energetic BIE method for 3D elastodynamics: The Dirichlet case. *Comput. Mech.* **2023**, *72*, 885–905. [CrossRef]
47. Coppolino, L.; Desiderio, L. Space-time energetic Galerkin BEM for the numerical solution of 3D elastodynamic problems: Overcoming challenges of the strongly singular integral operator. *Comput. Mech.* **2025**, *76*. [CrossRef]
48. Laursen, T.A. *Computational Contact and Impact Mechanics*; Springer: Berlin/Heidelberg, Germany, 2003. [CrossRef]

49. Chouly, F.; Hild, P.; Renard, Y. *Finite Element Approximation of Contact and Friction in Elasticity*; Birkhäuser: Cham, Switzerland, 2023. [CrossRef]
50. Eck, C.; Jarušek, J.; Krbec, M. *Unilateral Contact Problems: Variational Methods and Existence Theorems*; CRC Press: Boca Raton, FL, USA, 2005. [CrossRef]
51. Kashiwabara, T.; Itou, H. Unique solvability of a crack problem with Signorini-type and Tresca friction conditions in a linearized elastodynamic body. *Phil. Trans. R. Soc. A* **2022**, *380*, 20220225. [CrossRef]
52. Migórski, S.; Ochal, A.; Shillor, M.; Sofonea, M. Nonsmooth dynamic frictional contact of a thermoviscoelastic body. *Appl. Anal.* **2018**, *97*, 1228–1245. [CrossRef]
53. Hilber, H.M.; Hughes, T.J.R.; Taylor, R.L. Improved numerical dissipation for time integration algorithms in structural dynamics. *Earthq. Eng. Struct. Dyn.* **1977**, *5*, 283–292. [CrossRef]
54. Laursen, T.; Chawla, V. Design of energy conserving algorithms for frictionless dynamic contact problems. *Int. J. Numer. Methods Eng.* **1997**, *40*, 863–886. [CrossRef]
55. Kovtunenko, V.A.; Renard, Y. Convergence analysis of semi-smooth Newton method for mixed FEM approximations of dynamic two-body contact and crack problems. *J. Comput. Appl. Math.* **2025**, *471*, 116722. [CrossRef]
56. Kovtunenko, V.A.; Renard, Y. FEM approximation of dynamic contact problem for fracture under fluid volume control using HHT-α and semi-smooth Newton methods. *Appl. Numer. Math.* **2025**, *218*, 148–158. [CrossRef]
57. Itou, H.; Kovtunenko, V.; Rajagopal, K. Nonlinear model of a porous body with fluid-driven fracture under cohesion contact conditions and fluid volume control. *Math. Mod. Meth. Appl. Sci.* **2025**, *35*, 2311–2328. [CrossRef]
58. Kovtunenko, V.A. Space-time finite element based primal-dual active set method for the non-smooth problem of impact of rigid obstacle by elastic bar. *Comput. Math. Model.* **2025**. [CrossRef]
59. Kovtunenko, V.A. Space-time primal-dual active set method: Benchmark for collision of elastic bar with discontinuous velocity. *Computation* **2025**, *13*, 210. [CrossRef]